Applied Catalysis B: Environmental 184 (2016) 174–181

Contents lists available at ScienceDirect

Applied Catalysis B: Environmental

journal homepage: www.elsevier.com/locate/apcatb

Simultaneous excitation of $PdCl_2$ hybrid mesoporous g-C_3N_4 molecular/solid-state photocatalysts for enhancing the visible-light-induced oxidative removal of nitrogen oxides

Zizhong Zhang[a,b,*], Mukun Xu[a], Wingkei Ho[b,**], Xianwen Zhang[a], Zhenya Yang[a], Xuxu Wang[a]

[a] Research Institute of Photocatalysis, State Key Laboratory of Photocatalysis on Energy and Environment, Fuzhou University, Fuzhou 350002, China
[b] Department of Science and Environmental Studies, The Hong Kong Institute of Education, Hong Kong, China

ARTICLE INFO

Article history:
Received 24 August 2015
Received in revised form
15 November 2015
Accepted 22 November 2015
Available online 25 November 2015

Keywords:
mpg-CN
$PdCl_2$ hybrid
Z-scheme
NO removal
Photocatalysis

ABSTRACT

A simple and efficient molecular/solid-state hybrid photocatalyst consisting of noble metal (i.e., Au^{III}, Pt^{IV}, and Pd^{II}) chlorides-functionalized-mesoporous graphitic carbon nitride (mpg-CN) was developed to improve the photocatalytic performance of mpg-CN toward NO removal. Compared with the parent mpg-CN, the optimal 1% $PdCl_2$ modified mpg-CN increased the conversion efficiency by approximately 33%, improved the inhibiting efficiency of NO_2 release by approximately three times, and promoted the long term stability of photocatalysts for NO removal in a continuous flow model reaction system. The prepared samples were characterized by X-ray diffraction, transmission electron microscopy with energy-dispersive X-ray spectroscopy elemental mapping, ultraviolet–visible light absorbance spectroscopy, X-ray photoelectron spectroscopy, photoluminescence emission spectroscopy and electron paramagnetic resonance spectroscopy. The ultrafast charge separation and efficient generation of $O_2^{\bullet-}$ oxygen species were achieved by the charge transfer model of $PdCl_2$/mpg-CN similar to the solid-state Z-scheme system. This charge transfer model contributed to the high photocatalytic performance of the prepared $PdCl_2$/mpg-CN molecular/solid-state hybrid photocatalyst.

1. Introduction

Nitrogen oxides (NO*x*) released into the atmosphere from automobile exhausts and fossil fuel combustion are major air pollutants that trigger serious environmental problems, including acid rain, photochemical smog, and haze. Photocatalytic oxidation has received attention as a powerful and simple technology for NO*x* degradation [1–3]. TiO_2 is a commonly used photocatalyst for this reaction [4–6]. However, TiO_2 with large intrinsic band gap (3.2 eV for anatase and 3.0 eV for rutile) is active only under ultraviolet (UV) light (wavelength <400 nm). Thus, the high efficiency for solar light utilization of this catalyst is restricted [7].

Carbon nitride materials have recently attracted wide attention as noble meter-free and visible-light active photocatalysts; the capacity of these materials to produce H_2 is comparable with that of conventional inorganic materials [8–12]. Graphitic carbon nitride (g-C_3N_4) possesses high thermal and chemical stability with a medium band gap (2.7 eV) matching the suitable redox potentials. However, the photocatalytic oxidation of NO by g-C_3N_4 is slow because of the deactivation and fast recombination of photogenerated hole/electron pairs of block g-C_3N_4 [13,14]. Modification of g-C_3N_4 is indispensable to overcome these problems. For example, nanocasting with various silica templates was used to synthesize mesoporous g-C_3N_4 with high surface area. Metal or nonmetal doping, copolymerization, coupling with noble metal, dye sensitization and semiconductor hybridization were also developed to extend the visible light absorption and enhance the separation of hole/electron pairs of g-C_3N_4 [15–19]. Metal or nonmetal doping promotes visible-light photocatalytic activity, but this technique also causes thermal or crystal instability and increases carrier trapping [20]. This phenomenon may decrease the photocatalytic efficiency and limit the practical application of g-C_3N_4. Noble metal surface plasmon resonance mediated g-C_3N_4, which can adjust the absorption in solar spectra, is widely used for photocatalytic organic pollutant removal and water splitting. However, noble

* Corresponding author at: Research Institute of Photocatalysis, State Key Laboratory of Photocatalysis on Energy and Environment, Fuzhou University, Fuzhou 350002, China.
** Corresponding author.
E-mail addresses: z.zhang@fzu.edu.cn (Z. Zhang), keithho@ied.edu.hk (W. Ho).

http://dx.doi.org/10.1016/j.apcatb.2015.11.034
0926-3373/

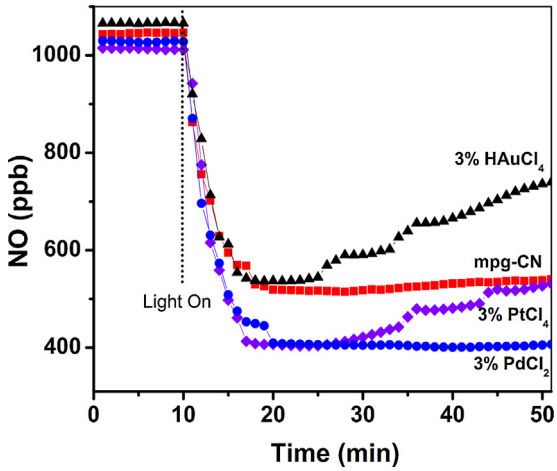

Fig. 1. Time-online data for NO removal over the parent mpg-CN and $HAuCl_4$, $PtCl_4$, or $PdCl_2$-modified samples.

metal-mediated materials are often irreversibly deactivated for NO*x* photocatalytic oxidation degradation [21].

Constructing heterostructures on g-C_3N_4 surface has emerged as an effective strategy to drive the separation and transfer of photogenerated electron–hole pairs and extend the light response of the photocatalyst because a wide range of available semiconductors can be selected [22–24]. For example, Yan et al. prepared a g-C_3N_4/TaON composite with higher activity than either a single phase of g-C_3N_4 or TaON in RhB photodegradation [25]. Solid-state junctions have attracted much attention, whereas molecular/solid-state heterojunctions remain largely unexplored for g-C_3N_4 matrix. A wide range of molecular catalysts, such as dye or Ru-based molecular, can be easily applied to form a semiconductor-molecule heterojunction for adjusting the redox property and facilitating charge separation.

In this paper, we report the surface functionalization of mesoporous g-C_3N_4 (mpg-CN) with a molecular catalyst, noble metal (i.e., Au^{III}, Pt^{IV}, and Pd^{II}) chlorides, to enhance NO*x* photocatalytic oxidation. Simultaneous excitation of $PdCl_2$/mpg-CN hybrid photocatalysts was achieved to improve charge separation and active oxygen species generation. This excitation contributed not only to the great enhancement of activity and suppression of toxic intermediate NO_2 release but also to the favorable stability for NO removal on the $PdCl_2$-modified mpg-CN samples.

2. Experimental

2.1. Samples preparation

Porous g-C_3N_4 was synthesized through urea polymerization using silica nanoparticles as the template. In a typical synthesis, 10 g of urea was first dissolved in 30 ml of de-ionic water and then added with 2 g of silica (5–15 nm size nanoparticles). The resulting suspension was stirred for 1 h at room temperature for complete mixing, heated to 60 °C for drying, and then ground into fine powder. The SiO_2/urea composite was placed in a crucible with a cover and then heated at 5 °C min^{-1} up to 550 °C for 4 h in a muffle. To remove the silica template, the SiO_2/g-C_3N_4 composite was soaked in 250 ml of NH_4HF_2 (4 M) aqueous solution for 1 day without stirring. The resulting solids were recovered through filtration, washed with water several times, and then dried at 60 °C overnight to obtain pale-yellow powders of porous g-C_3N_4.

Porous g-C_3N_4 samples with metal (i.e., Au^{III}, Pt^{IV}, and Pd^{II}) chlorides were prepared using a simple impregnation method. Approximately 0.5 g of porous g-C_3N_4 powders were added to an aqueous solution containing an appropriate amount of metal chloride and then ultrasonically mixed for 20 min. The dispersion was heated in a water bath at 60 °C to vaporize water. The resultant powders were further dried overnight in an oven at 60 °C. As a comparison, Pd metal-loaded porous g-C_3N_4 powders were prepared by using 12% sodium borohydride solution to reduce the corresponding $PdCl_2$-sensitized porous g-C_3N_4 powders.

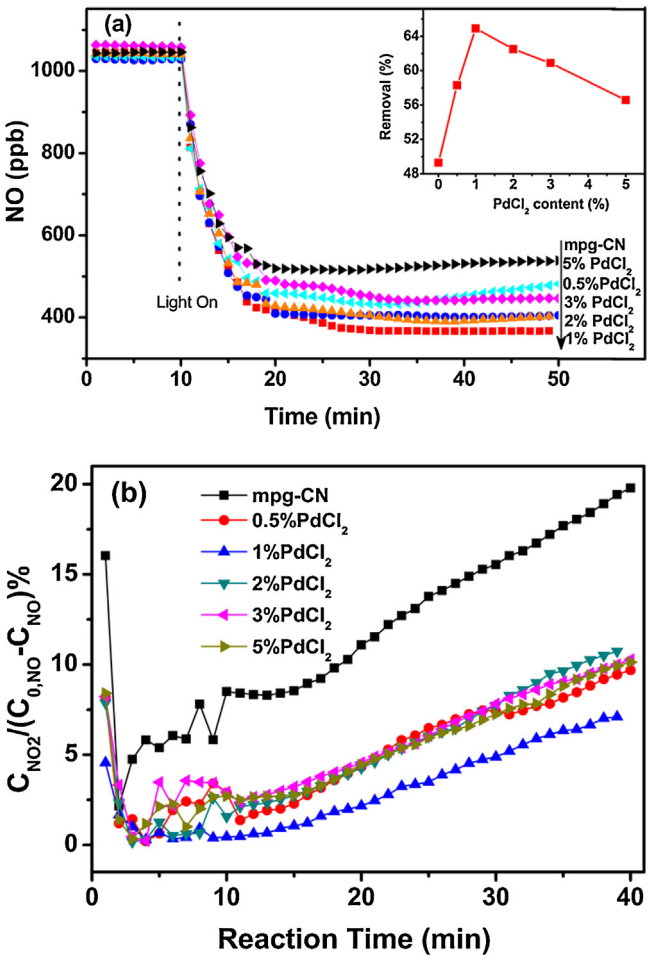

Fig. 2. Time-course of NO concentration (a) and release efficiency of NO_2 (b) over various contents of $PdCl_2$-modified mpg-CN.

2.2. Characterization

X-ray diffraction (XRD) measurements were performed on a Bruker D8 Advance X-ray diffractometer with Cu$K\alpha_1$ radiation (λ = 1.5406 Å). Brunauer–Emmett–Teller (BET) measurements were conducted using a Micrometrics ASAP 2020 surface area/porosity analyzer. UV–vis spectra were recorded on a Varian Cary 500 Scan UV–vis-near-infrared (NIR) spectrophotometer by using a $BaSO_4$ standard. Electron paramagnetic resonance (EPR) spectra were recorded at room temperature by using a Bruker A-300-EPR X-band spectrometer. X-ray photoelectron spectroscopy (XPS) spectroscopy was conducted on a VG ESCALAB 250 XPS system with a monochromatized Al Ka X-ray source (15 kV, 200 W, 500 μm pass energy = 20 eV). All binding energies were referenced to the C 1s peak at 284.6 eV of surface adventitious carbon. Photoluminescence (PL) emission spectra were recorded at 350 nm excitation on an Edinburgh Analytical Instruments FL/FSTCSP920 spectrometer. Transmission electron microscopy (TEM) was performed using a JEOL model JEM 2010 EX instrument at an accelerating voltage of 200 kV.

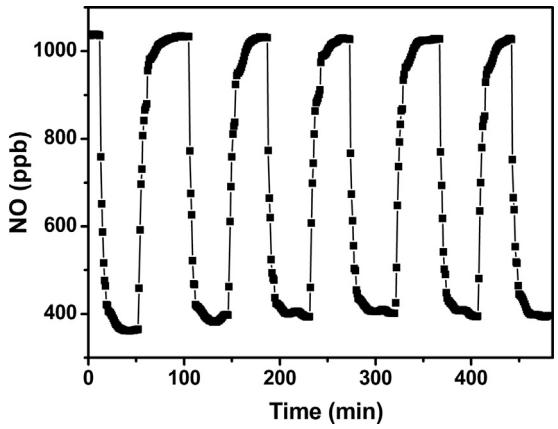

Fig. 3. Prolonged stability of the optimal 1% $PdCl_2$/mpg-CN catalysts for NO removal.

2.3. Photocatalytic measurements

Photocatalytic activity was measured through NO removal at approximately 1100 ppb levels in a continuous flow reactor at ambient temperature. The volume of the rectangular reactor, which is made of stainless steel and covered with quartz glass window, was 4.5 L (30 cm × 15 cm × 10 cm). A 30 W visible light-emitting diode as a light source was vertically placed outside the reactor. A dish with a diameter of 12.0 cm was coated with the photocatalyst (0.2 g) and then pretreated at 70 °C to remove water in the suspension. NO gas was acquired from a compressed gas cylinder at a concentration of 50 ppm of NO (N_2 balance) and diluted to approximately 1100 ppb by using a dynamic gas calibrator (Ecotech GasCal 1000) in combination with a zero air supply. The gas flow rate through the reactor was controlled at 1000 ml min^{-1} by using a mass flow controller. After achieving the adsorption–desorption equilibrium, the lamp was turned on. The concentration of NO was continuously measured using a NO*x* analyzer model T200 (Teledyne API). The removal ratio (δ) of NO was calculated as $\delta(\%) = (1 - C/C_0) \times 100$, where C_0 is the initial concentration of NO and C is the concentration of NO after photocatalytic reaction.

3. Results and discussion

3.1. Photocatalytic activity

Fig. 1 shows the effect of various metal (i.e., Au, Pt, and Pd) chlorides on the photocatalytic performance of the modified mpg-CN toward NO removal in a continuous flow model. Under visible light irradiation, NO concentrations were rapidly reduced at initial time over all the photocatalyst samples, but the photocatalytic activity varied with the different metal chloride complexes. Compared with the parent mpg-CN, the $HAuCl_4$-modified mpg-CN slightly decreased the photocataytic activity and caused a distinct deactivation after 15 min of initial reaction. $PtCl_4$ modification effectively increased NO removal at the initial stage of reaction, but caused gradual deactivation with prolonged time. Interestingly, the $PdCl_2$-modified samples improved the efficiency and maintained the stability of the photocatalysts for NO removal. The poor stability of the $HAuCl_4$ and $PtCl_4$-modified samples may be attributed to the photoreduction of metal ions to metallic states [26]. The color of $PtCl_4$/mpg-CN samples changed from light yellow to brownish yellow after photocatalytic reaction, indicating the reduction of $PtCl_4$. When we prepared the metallic Pt modified mpg-CN samples and employed them for the photocatalytic removal of NO, it was found that Pt/mpg-CN samples exhibited a distinct deactivation with reaction time (see Fig. S1). This suggests that the photoreduction of $HAuCl_4$ and $PtCl_4$ on mpg-CN accounted for the deactivation toward NO removal. Metallic Pd-modified mpg-CN samples were also used to study the impact of chemical states on the photocatalytic activity. Metallic Pd induced both low activity and deactivation for NO removal (see Fig. S2). This indicates that $PdCl_2$ is sufficiently stable in keeping 2+ chemical states and is very important for the high photocatalytic activity of $PdCl_2$/mpg-CN samples. The stability of $PdCl_2$ will be verified by XPS analysis later in this paper.

We examined the photocatalytic activity during NO removal as a function of $PdCl_2$ content. Fig. 2A shows the time course of NO concentration over various contents of $PdCl_2$-modified mpg-CN. The $PdCl_2$/mpg-CN samples significantly improved the photocatalytic capability of mpg-CN. However, the final degraded level of NO removal depended on the $PdCl_2$ contents of mpg-CN. The parent mpg-CN displayed approximately 49% NO removal at steady state. The NO removal rapidly increased upon $PdCl_2$ modification and reached the maximum with 1% $PdCl_2$. Approximately 65% of NO was removed over 1% $PdCl_2$/mpg-CN, which enhanced the conversion efficiency by approximately 33% as compared with the parent mpg-CN samples. NO removal gradually decreased as $PdCl_2$ content was increased from 2% to 5%. Therefore, 1% $PdCl_2$ was the optimum content for modifying mpg-CN and obtaining the highest photocatalytic activity towards NO removal.

In general, the photocatalytic oxidative removal of NO in air consists of two main processes: oxidation of NO to NO_2 and subsequent oxidation of NO_2 to NO_3^- [27]. The reaction intermediate of NO_2 is more toxic than the original NO. Therefore, the release of NO_2 to gas phase should be suppressed. The intermediate of NO_2 con-

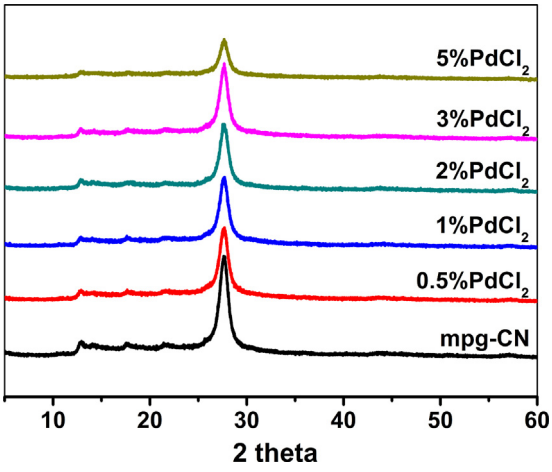

Fig. 4. XRD patterns of the various $PdCl_2$-modified mpg-CN samples.

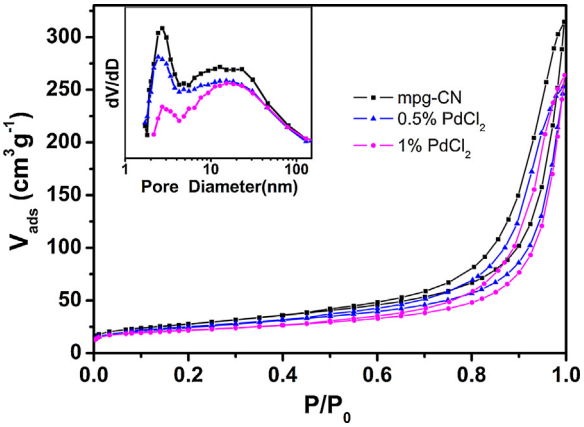

Fig. 5. N_2 adsorption–desorption isotherms and pore size distribution (inset) of the parent mpg-CN and 0.5% or 1% $PdCl_2$-modified samples.

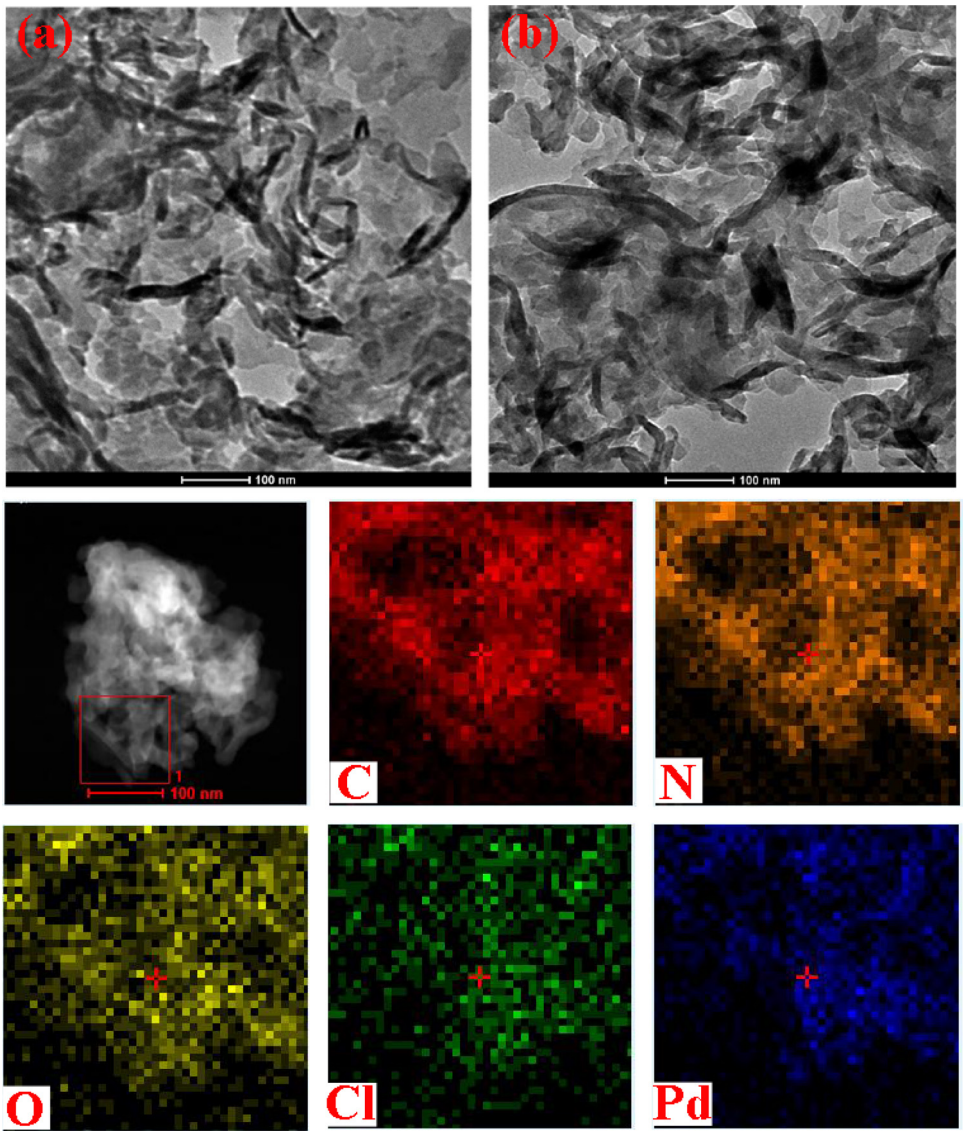

Fig. 6. TEM images of the parent mpg-CN (a) and 1% $PdCl_2$-modified samples (b), together with the EDS elemental mapping analysis of 1% $PdCl_2$/mpg-CN hybrid samples.

centration during the NO removal was also monitored. We used the detected NO_2 concentration (C_{NO_2}) divided by the degraded amount of NO ($C_{0,NO}$–C_{NO}) at every reaction point to represent the release efficiency of NO_2 over each photocatalyst sample (Fig. 2B). The amount of NO_2 product was increased with prolonging reaction time for all samples. After 40 min of reaction, approximately 20% of NO_2 was released from the parent mpg-CN samples. However, the release of NO_2 was dramatically depressed in the case of $PdCl_2$, especially for 1% $PdCl_2$. Approximately 7% of NO_2 was released from 1%$PdCl_2$ samples after 40 min of reaction; this value was approximately 1/3 that of the NO_2 amount released from the parent mpg-CN. This result indicates that the 1% $PdCl_2$-hybrid sample increased the inhibiting efficiency of NO_2 release by approximately three times compared with the parent mpg-CN. Hence, the optimal 1% $PdCl_2$ modification not only greatly enhanced the photocatalytic oxidative removal of NO but also efficiently suppressed the release of toxic intermediate NO_2. $PdCl_2$ modification may increase the number of active sites or enhance the separation of photogenerared charge on mpg-CN samples, which is beneficial for the conversion of NO_2 into NO_3^-. Therefore, the NO removal efficiency was improved on $PdCl_2$-modified mpg-CN samples. Thus, we can expect a good stability of 1% $PdCl_2$/CN for the photocatalytic oxidative removal of NO. The long-term stability of photocatalysts for NO removal was evaluated (Fig. 3). The NO removal activity of the 1% $PdCl_2$/CN samples remained high even after six cycles of repeated runs.

3.2. Structural characterization and chemical states

Fig. 4 shows the XRD patterns of the $PdCl_2$/mpg-CN composite samples. All of the samples exhibited similar diffraction patterns with the typical g-C_3N_4 structure. No residual SiO_2 was observed in mpg-CN after NH_4HF_2 corrosion. The strong diffraction peak at 27.6° corresponding to an interplanar distance of approximately 0.323 nm was characterized for (0 0 2) reflection of graphitic layered materials, whereas the weak one at 12.8° (d = 0.691 nm) for (1 0 0) reflection can be attributed to the in-plane structural packing motif of tri-*s*-triazine units. The $PdCl_2$ surface-modified samples displayed no diffraction peaks assignable to palladium chloride, indicating the fine dispersion of chlorides on the surface of mpg-CN. The intensity of the peak for the (0 0 2) reflection was decreased, suggesting that ultrasonic crashing decreased the content of layered structure [28]. The N_2 adsorption–desorption isotherms of the samples were measured to understand the textural properties (Fig. 5). N_2 isotherms revealed a pronounced hysteresis loop typi-

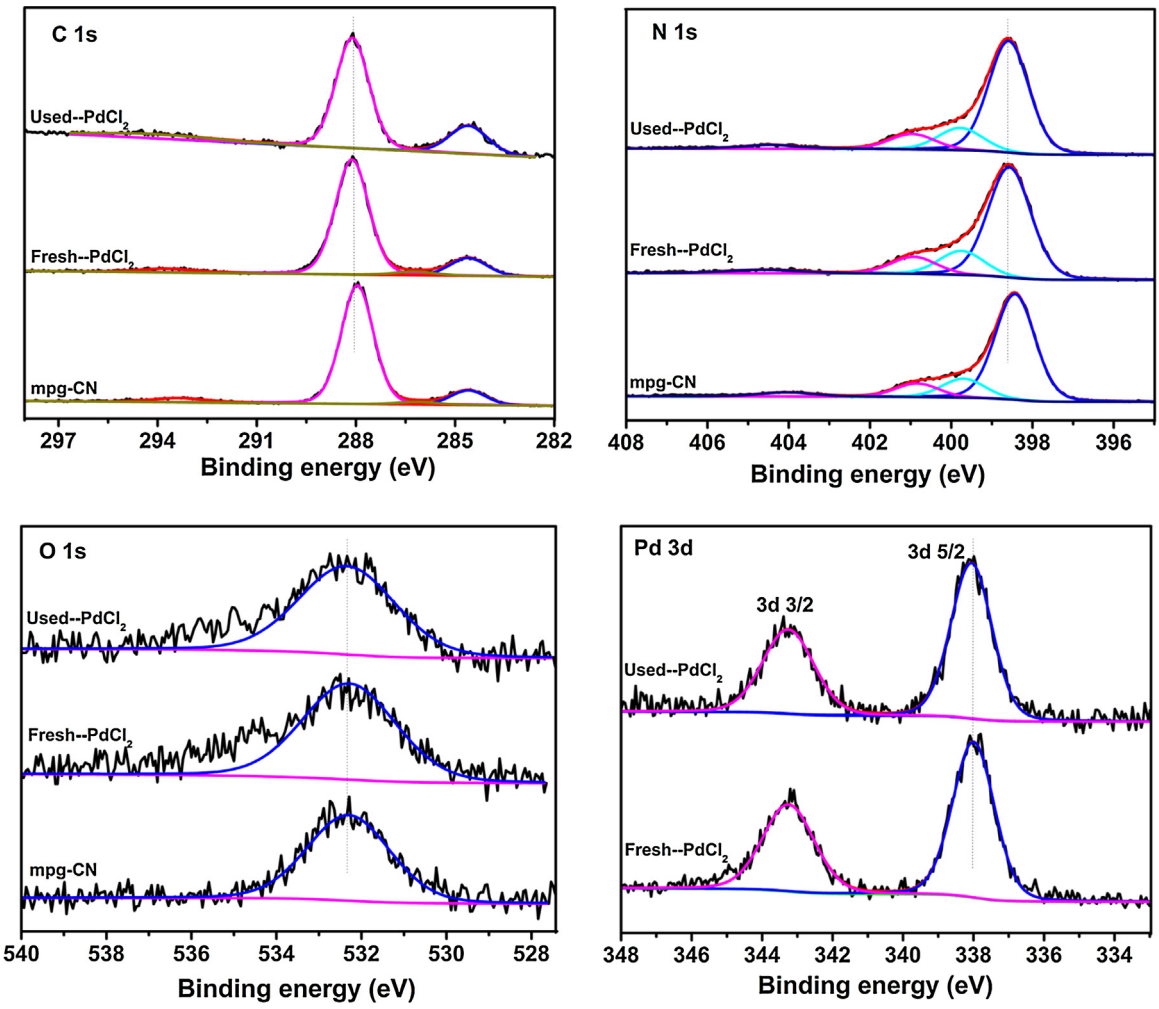

Fig. 7. XPS spectra of mpg-CN and 1% $PdCl_2$/mpg-CN before or after the prolonged photocatalytic reaction.

cal for the presence of mesoporous structures caused by the SiO_2 template. The pore size distribution plot shows two pore sizes at 2.7 and 18.1 nm for mpg-CN samples (Fig. 5, inset). The BET surface area and pore volumes are summarized in Table 1. $PdCl_2$ surface modification slightly decreased the BET surface area and pore volumes, because $PdCl_2$ was adsorbed inside the pore to block N_2 uptake, as indicated by the decrease in pore size at 2.7 nm with the increase in $PdCl_2$ contents (Fig. 5, inset).

The microstructure of mpg-CN and $PdCl_2$/mpg-CN was further revealed by TEM observations (Fig. 6). The as-prepared mpg-CN samples appeared as aggregates of thin sheet-like mass. Mesoporous structure from the removal of SiO_2 templates was retained around thin layers as indexed. The porous structure increased the surface to volume ratio and the reactive site number, both of which enhanced the photocatalytic activity of mpg-CN. However, $PdCl_2$ modification exerted no influence on the microstructure of mpg-CN. The element compositions and their distributions on the $PdCl_2$/mpg-CN composite were examined through energy-dispersive X-ray spectroscopy (EDS) elemental mapping. As shown in Fig. 6, the elements C, N, Cl and Pd were detected and homogeneously distributed on the surface of the entire composite matrices. These results verify the adsorption of $PdCl_2$ on the mpg-CN surface. The TEM image together with EDS mapping of $PdCl_2$/mpg-CN after prolonged reaction was also performed, as shown in Fig. S3. We can find that the elements C, N, Cl and Pd were also detected and homogeneously distributed on the sample surface. This confirms the stability of $PdCl_2$/mpg-CN for NO removal.

Fig. 7 shows the XPS spectra to determine the chemical states of C, N, and Pd in mpg-CN and $PdCl_2$/mpg-CN. For the parent mpg-CN, the main core level peak of the C 1s XPS is localized at 287.9 eV, which can be ascribed to the sp^2 carbon—nitrogen bonding of the aromatic ring system [29]. The N 1S spectra can be fitted into three peaks at 398.4, 399.7, and 400.8 eV, which correspond to N bonded to carbon atoms (C=N—C) of triazine rings, the tertiary N in the form of N—$(C)_3$, and amino functional groups (C—N—H) [30], respectively. A weak O1s peak at 532.3 eV was also detected and can be attributed to the adsorbed O_2 [31]. The binding energies of C 1s and N 1S spectra is shifted to higher levels by 0.2 eV as $PdCl_2$ surface modification in comparison with the parent mpg-CN, indicating the interactions between $PdCl_2$ and mpg-CN. This result can be ascribed to the fact

Table 1
BET specific surface area and pore volume of the prepared samples.

Sample	mpg-CN	0.5% $PdCl_2$	1% $PdCl_2$	2% $PdCl_2$	3% $PdCl_2$	5% $PdCl_2$
BET ($m^2\ g^{-1}$)	97.4	85.2	84.8	85.7	79.6	73.9
Pore volume ($cm^3\ g^{-1}$)	0.486	0.388	0.405	0.425	0.445	0.465

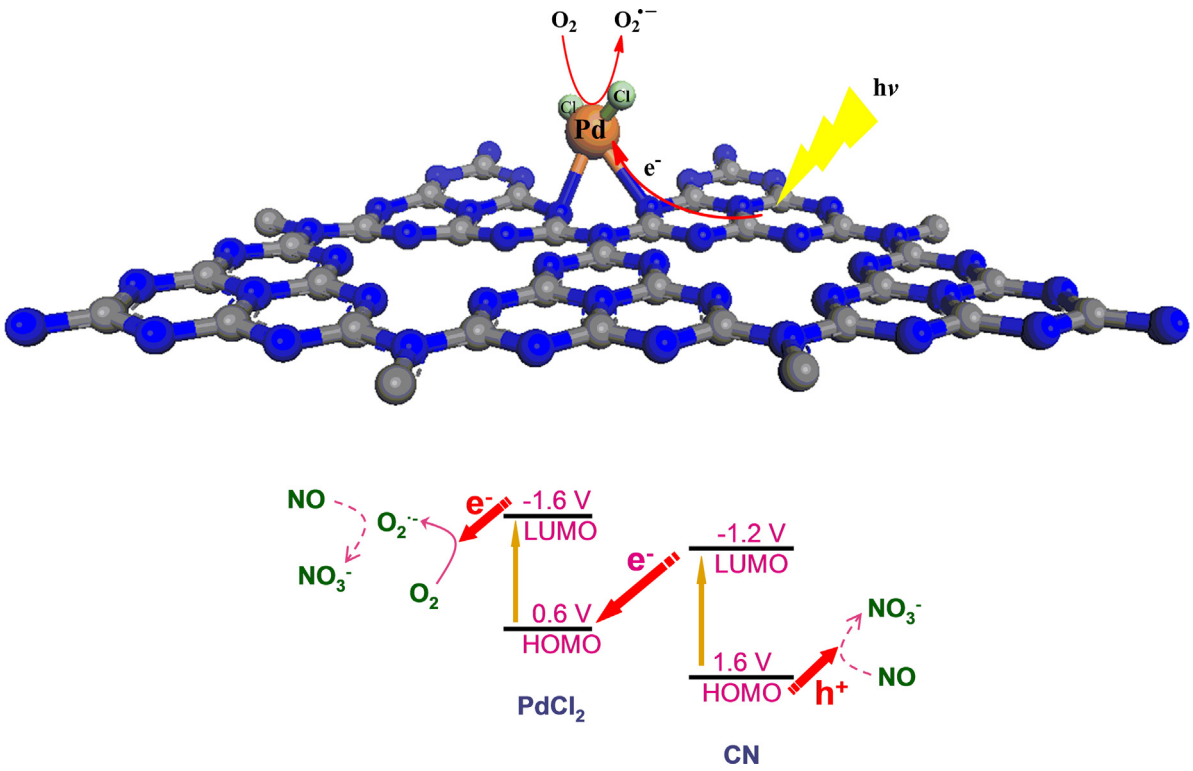

Scheme 1. Possible photocatalytic mechanism of $PdCl_2$/mpg-CN molecular/solid-state hybrid photocatalyst under visible light irradiation.

that the coordination complex between Pd^{2+} ions and donor N in triazine rings decreases the electron density of triazine rings and thus shifts the binding energies of C 1s and N 1S to higher levels [32]. The Pd 3d XPS spectra of $PdCl_2$/mpg-CN consist of two peaks at 338.0 and 343.2 eV, which correspond to Pd 3d5/2 and Pd 3d3/2, respectively, and can be assigned to Pd^{2+} from $PdCl_2$ adsorbed on the surface of mpg-CN [33]. The actual content of $PdCl_2$ was calculated to be 1.2 at% on the sample surface from XPS spectra. This value is higher than the added amount for the nominal 1% $PdCl_2$/g-C_3N_4 composite. This can be explained by the fact that the $PdCl_2$ was not diffused into the interior of g-C_3N_4 but only adsorbed on the surface. The XPS spectra of pure $PdCl_2$ were performed, as shown in Fig. S4. Comparison with the pure $PdCl_2$ samples, $PdCl_2$-CN samples displays the binding energy of Pd 3d5/2 at 338.0 eV, which is higher than that for pure $PdCl_2$ by 0.2 eV. This confirms the coordination complex between $PdCl_2$ and CN in hybrid samples. The used $PdCl_2$/mpg-CN displayed almost the same Pd 3d XPS spectra as the fresh $PdCl_2$/mpg-CN samples in the chemical state of Pd^{2+} even after six runs of NO removal reaction. No peaks associated with metallic Pd were observed in the used samples. The sustainment of Pd^{2+} chemical states is of significant importance and accounts for the high stability and good performance of the $PdCl_2$/mpg-CN samples for photocatalytic NO removal.

3.3. Optical properties

Fig. 8 shows the UV–vis absorption spectra of mpg-CN hybrid with various contents of $PdCl_2$. The unmodified mpg-CN exhibited a sharp band edge absorption at ca. 460 nm with a long and broad absorption shoulder extending into 600 nm. This absorption feature is typical for g-C_3N_4 materials prepared through thermal polymerization [34]. The tail absorption above 460 nm arises from the presence of intrinsic defect in mpg-CN samples [35]. With $PdCl_2$ species chemisorbed on the surface of mpg-CN, the

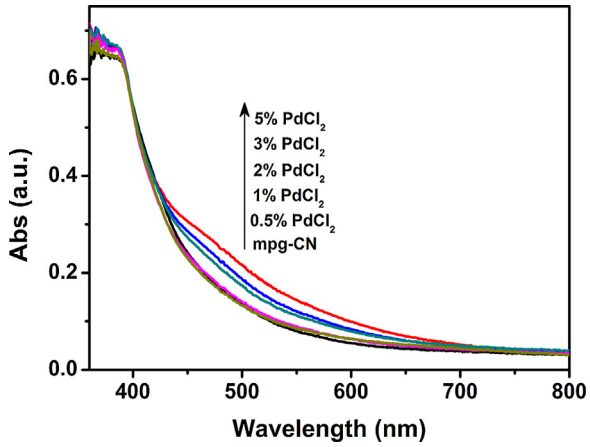

Fig. 8. UV–vis absorption spectra of mpg-CN hybrid with various contents of $PdCl_2$.

absorption shoulder band above 460 nm increased with increasing $PdCl_2$ contents. This result can be attributed to the absorption of the ligand-to-metal charge-transfer band of $PdCl_2$ centers [36]. Thus, $PdCl_2$ modification can improve the ability of mpg-CN to harvest more visible light. Moreover, simultaneous excitation of both mpg-CN and $PdCl_2$ probably occurs on $PdCl_2$/mpg-CN under visible light irradiation to enhance its photocatalytic performance. PL measurements were conducted to determine whether or not $PdCl_2$ surface modification can suppress the recombination of photogenerated electron and hole on mpg-CN (Fig. 9). Evidently, $PdCl_2$ modification substantially quenched the PL of mpg-CN, indicating enhancement of the separation of charge carriers. The order of PL quenching for the samples with different $PdCl_2$ contents was quite in parallel with their photocatalytic activity results reported above. 1% $PdCl_2$/g-C_3N_4 samples displayed the lowest PL intensity and thus the highest efficiency for the separation of

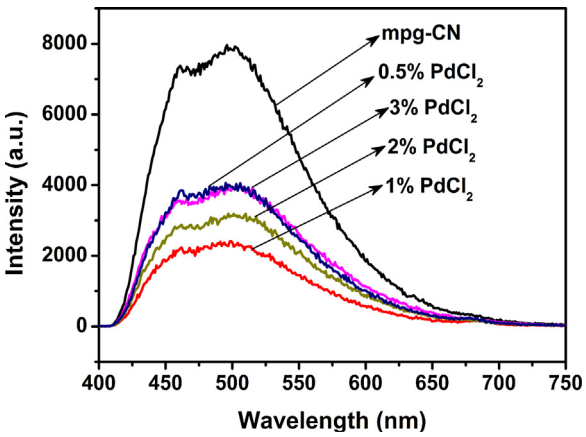

Fig. 9. PL emission spectra of the various $PdCl_2$-modified mpg-CN samples.

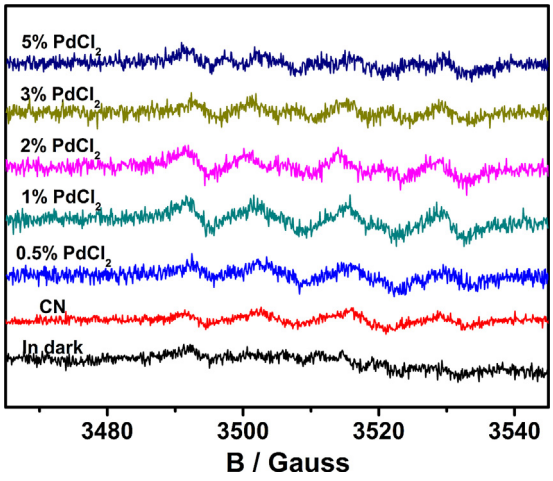

Fig. 10. Formation of $^{\bullet}OOH/O_2^{\bullet-}$ radicals determined by DMPO spin-trapping EPR in methanol solutions under visible irradiation over various $PdCl_2$-modified mpg-CN samples.

photogenerated charge. Therefore, 1% $PdCl_2$/g-C_3N_4 showed the highest photocatalytic activity and stability for NO removal.

3.4. Mechanism

Photocatalytic NO removal in air to NO_3^- products is an oxidative process involving active oxygen species. EPR with the spin trapping agents 5,5-dimethyl1-pyrroline *N*-oxide (DMPO) was used to determine the active oxygen species including $O_2^{\bullet-}$ and $HO^{\bullet}$ involved in the reaction and reveal the reaction mechanism. Fig. 10 shows the EPR spectra of DMPO radical adducts over various $PdCl_2$/mpg-CN under visible light ($\lambda \geq 420$ nm) irradiation. No EPR signals for DMPO-$^{\bullet}OH$ adducts appeared under visible light illumination, indicating that no $^{\bullet}OH$ radicals were produced. This result can be attributed to the fact that the +1.99 eV redox potential of $HO^{\bullet}/HO^-$ and approximately +1.6 eV valence band (VB) potential of CN or +0.6 eV HOMO potential of $PdCl_2$ are not sufficiently positive to generate $HO^{\bullet}$ [37,38]. However, the EPR signals for the typical DMPO-$^{\bullet}OOH/O_2^{\bullet-}$ adducts (Fig. 10) were observed on the different $PdCl_2$/mpg-CN samples upon visible light irradiation. The intensity of the produced $O_2^{\bullet-}$ species varied with $PdCl_2$ content. The 1% $PdCl_2$/mpg-CN catalysts displayed a maximum concentration of $O_2^{\bullet-}$ species. The order of the amount of $O_2^{\bullet-}$ species produced on the different $PdCl_2$/mpg-CN samples agreed with the photocatalytic activity results for NO oxidation. These results indicate that the active oxygen species $O_2^{\bullet-}$ radicals acted as the major oxidative species responsible for the oxidative removal of NO on the $PdCl_2$/mpg-CN catalysts. The more amount of the active oxygen $O_2^{\bullet-}$ species generated on 1% $PdCl_2$/mpg-CN account for its higher photocatalytic activity for NO removal. Besides $O_2^{\bullet-}$ species, photogenerated holes on g-C_3N_4 also play an importance role in the photocatalytic NO removal, as indicated in the early reports by Dong et al. [39]. The excited holes in mpg-CN can also directly oxidize NO.

It has been reported by Kisch et al. [40] that local excitation of the metal chloride complex (MCl_n, M = Pt, Rh, Pd et al.) loaded on TiO_2 particles under visible light irradiation yields a ligand-to-metal charge-transfer state, producing a reduced species (MCl_{n-1}) and Cl radical. The reduced species (MCl_{n-1}) then rapidly transfers an electron (e^-) to the conduction band of titania where this electron is captured by O_2 to generate $O_2^{\bullet-}$ species for the photodegradation of organic pollutants. In these MCl_n hybrid TiO_2 systems, the TiO_2 matrix is inactive under visible light and works as a charge trap for the electronically excited MCl_n component. When the simultaneous excitation of MCl_n and TiO_2 was conducted with a UV light, MCl_n reduced the photocatalytic activity of the TiO_2 matrix because of the inner filter effect of the metal complex for diminishing the band-to-band excitation of TiO_2 [41]. For the $PdCl_2$/mpg-CN samples, both $PdCl_2$ and mpg-CN can be excited by visible light. However, the photocatalytic activity of mpg-CN was greatly improved by the $PdCl_2$ complex hybrid. This result reveals a different reaction mechanism of $PdCl_2$/mpg-CN catalyst from that of $PdCl_2/TiO_2$. Apparently, the $PdCl_2$ hybrid can efficiently suppress the photogenerated charge recombination of mpg-CN when both $PdCl_2$ and mpg-CN are active under visible light irradiation, as proven by PL (Fig. 9). Moreover, the LUMO of $PdCl_2$ (−1.6 eV) is more negative than the conduction band edge of CN (−1.2 eV) [38]. Thus, the excited electron transfer from the conduction band of CN to the LUMO of $PdCl_2$ is energetically unfavorable, but the excited electron of CN transferred to the HOMO level of $PdCl_2$ is feasible for the charge separation. This charge transfer model is similar to that happened on $PtCl_x$/N-TiO_2 as reported by Higashimoto et al. [42].

A possible mechanism for the $PdCl_2$/mpg-CN catalyst of photoinduced charge separation and conversion is depicted in Scheme 1. Under visible light irradiation, both CN and $PdCl_2$ were simultaneously excited. The excited holes tended to keep in the VB (+1.6 V) of CN to directly oxidize NO, while the excited electrons from the CB (−1.2 V) of CN transferred to the HOMO level (+0.6 V) of $PdCl_2$. The electrons in the HOMO of $PdCl_2$ were further excited to its LUMO (−1.6 V), which were captured by the pre-adsorbed O_2 to produce the superoxide $O_2^{\bullet-}$ radicals, as evidenced by EPR spectroscopy. The above charge transfer mode is similar to that in the Z-scheme photocatalytic system [43]. This model leads to efficient charge separation and effectively suppresses the recombination of photoinduced electrons and holes in CN. Therefore, the CN hybrid with $PdCl_2$ complex exhibits an efficient photocatalytic activity for NO removal.

4. Conclusions

Surface functionalization of mpg-CN with $PdCl_2$ complex can greatly enhance the activity and stability for NO removal and suppress the release of the toxic intermediate NO_2 through the formation of a molecular/solid-state hybrid photocatalyst. Both $PdCl_2$ complex and mpg-CN matrix can be excited under visible light irradiation to produce charge carriers. The charge-transfer model similar to the solid-state Z-scheme system is formed on $PdCl_2$/mpg-CN and results in the ultrafast charge separation and efficient generation of $O_2^{\bullet-}$. These results contribute to the excellent photocatalytic performance of $PdCl_2$/mpg-CN. This work provides

a simple and efficient $PdCl_2$/mpg-CN hybrid photocatalyst with simultaneous excitation behavior for efficient NO removal.

Acknowledgments

This work was financially supported by the National Natural Science Foundation of China (Grant Nos. 21203029 and U1305242), the Natural Science Foundation of Fujian Province of PR China (2013J05024), and the Technology Project of Education Office of Fujian Province of PR China (JA12036 and JA14030). This research was also financially supported by the research grant of Early Career Scheme(ECS 809813) from the Research Grant Council, Hong Kong SAR Government, Internal Research Grant (R3588) and (R3633) from The Hong Kong Institute of Education.

Appendix A. Supplementary data

Supplementary data associated with this article can be found, in the online version, at http://dx.doi.org/10.1016/j.apcatb.2015.11.034.

References

[1] J. Lasek, Y.-H. Yu, J.C.S. Wu, J. Photochem. Photobiol. C: Photochem. Rev. 14 (2013) 29–52.
[2] C.H. Ao, S.C. Lee, Appl. Catal. B: Environ. 44 (2003) 191–205.
[3] Z. Ai, W. Ho, S. Lee, L. Zhang, Environ. Sci. Technol. 43 (2009) 4143–4150.
[4] J.S. Dalton, P.A. Janes, N.G. Jones, J.A. Nicholson, K.R. Hallam, G.C. Allen, Environ. Pollut. 120 (2002) 415–422.
[5] J. Ma, H. Wu, Y. Liu, H. He, J. Phys. Chem. C 118 (2014) 7434–7441.
[6] C.L. Bianchi, C. Pirola, F. Galli, G. Cerrato, S. Morandi, V. Capucci, Chem. Eng. J. 261 (2015) 76–82.
[7] M.R. Hoffmann, S.T. Martin, W. Choi, D.W. Bahnemann, Chem. Rev. 95 (1995) 69–96.
[8] X. Wang, K. Maeda, A. Thomas, K. Takanabe, G. Xin, J.M. Carlsson, K. Domen, M. Antonietti, Nat. Mater. 8 (2009) 76–80.
[9] X. Wang, S. Blechert, M. Antonietti, ACS Catal. 2 (2012) 1596–1606.
[10] J. Liu, Y. Liu, N. Liu, Y. Han, X. Zhang, H. Huang, Y. Lifshitz, S.-T. Lee, J. Zhong, Z. Kang, Science 347 (2015) 970–974.
[11] S. Yang, Y. Gong, J. Zhang, L. Zhan, L. Ma, Z. Fang, R. Vajtai, X. Wang, P.M. Ajayan, Adv. Mater. 25 (2013) 2452–2456.
[12] X. Xia, N. Deng, B. Tang, J. Xie, X. Shi, Y. Zhao, Q. Wang, W. Wang, B. Tang, Chem. Commun. 51 (2015) 10899–10902.
[13] T. Sano, S. Tsutsui, K. Koike, T. Hirakawa, Y. Teramoto, N. Negishi, K. Takeuchi, J. Mater. Chem. A 1 (2013) 6489–6496.
[14] W. Ho, Z. Zhang, M. Xu, X. Zhang, X. Wang, Y. Huang, Appl. Catal. B: Environ. 179 (2015) 106–112.
[15] C. Pan, J. Xu, Y. Wang, D. Li, Y. Zhu, Adv. Funct. Mater. 22 (2012) 1518–1524.
[16] J. Hong, X. Xia, Y. Wang, R. Xu, J. Mater. Chem. 22 (2012) 15006–15012.
[17] S. Cao, J. Yu, J. Phys. Chem. Lett. 5 (2014) 2101–2107.
[18] M. Shalom, S. Inal, C. Fettkenhauer, D. Neher, M. Antonietti, J. Am. Chem. Soc. 135 (2013) 7118–7121.
[19] W. Ho, Z. Zhang, W. Lin, S. Huang, X. Zhang, X. Wang, Y. Huang, ACS Appl. Mater. Interfaces 7 (2015) 5497–5505.
[20] L. Jing, W. Zhou, G. Tian, H. Fu, Chem. Soc. Rev. 42 (2013) 9509–9549.
[21] H. Wang, Z. Wu, Y. Liu, Y. Wang, Chemosphere 74 (2009) 773–778.
[22] F. Dong, Z. Zhao, T. Xiong, Z. Ni, W. Zhang, Y. Sun, W.-K. Ho, ACS Appl. Mater. Interfaces 5 (2013) 11392–11401.
[23] M. Xu, L. Han, S. Dong, ACS Appl. Mater. Interfaces 5 (2013) 12533–12540.
[24] J. Yu, S. Wang, J. Low, W. Xiao, Phys. Chem. Chem. Phys. 15 (2013) 16883–16890.
[25] S.C. Yan, S.B. Lv, Z.S. Li, Z.G. Zou, Dalton. Trans. 39 (2010) 1488–1491.
[26] C.-H. Huang, I.K. Wang, Y.-M. Lin, Y.-H. Tseng, C.-M. Lu, J. Mol. Catal. A: Chem. 316 (2010) 163–170.
[27] K. Hashimoto, K. Sumida, S. Kitano, K. Yamamoto, N. Kondo, Y. Kera, H. Kominami, Catal. Today 144 (2009) 37–41.
[28] K. Li, Z. Zeng, L. Yan, S. Luo, X. Luo, M. Huo, Y. Guo, Appl. Catal. B: Environ. 165 (2015) 428–437.
[29] J. Li, B. Shen, Z. Hong, B. Lin, B. Gao, Y. Chen, Chem. Commun. 48 (2012) 12017–12019.
[30] S. Wang, C. Li, T. Wang, P. Zhang, A. Li, J. Gong, J. Mater. Chem. A 2 (2014) 2885–2890.
[31] Z. Zhang, J. Long, X. Xie, H. Zhuang, Y. Zhou, H. Lin, R. Yuan, W. Dai, Z. Ding, X. Wang, X. Fu, Appl. Catal. A: Gen. 425–426 (2012) 117–124.
[32] X. Wang, X. Chen, A. Thomas, X. Fu, M. Antonietti, Adv. Mater. 21 (2009) 1609–1612.
[33] M.C. Militello, S.J. Simko, Surf. Sci. Spectra 3 (1994) 402–409.
[34] T. Tyborski, C. Merschjann, S. Orthmann, F. Yang, M.C. Lux-Steiner, S.-N. Th, J. Phys.: Condens Mater. 24 (2012) 162201.
[35] P. Niu, L.-C. Yin, Y.-Q. Yang, G. Liu, H.-M. Cheng, Adv. Mater. 26 (2014) 8046–8052.
[36] H.-F. Wang, W.E. Kaden, R. Dowler, M. Sterrer, H.-J. Freund, Phys. Chem. Chem. Phys. 14 (2012) 11525–11533.
[37] X. Yao, X. Liu, X. Hu, ChemCatChem 6 (2014) 3409–3418.
[38] E.F. Penka, C.W. Schläpfer, M. Atanasov, M. Albrecht, C. Daul, J. Organomet. Chem. 692 (2007) 5709–5716.
[39] G. Dong, W. Ho, Y. Li, L. Zhang, Appl. Catal. B: Environ. 174 (2015) 477–485.
[40] H. Kisch, L. Zang, C. Lange, W.F. Maier, C. Antonius, D. Meissner, Angew. Chem. Int. Ed. 37 (1998) 3034–3036.
[41] W. Macyk, H. Kisch, Chem. Eur. J. 7 (2001) 1862–1867.
[42] S. Higashimoto, K. Takamatsu, M. Azuma, M. Kitano, M. Matsuoka, M. Anpo, Catal. Lett. 122 (2008) 33–36.
[43] K. Maeda, ACS Catal. 3 (2013) 1486–1503.